DOI 10.5162/sensoren2024/C1.2

A guideline for the fabrication of fully 3D-printed torque sensor elements - demonstrated based on a real example

Lukas Stiglmeier [1], Nikolai Hangst [1], Philipp Gawron [1], Thomas M. Wendt [1], and Stefan J. Rupitsch [2],

[1] Hochschule Offenburg, Fakultät Wirtschaft, Work-Life Robotics Institute, Halle 101, Max-Planck-Straße 1, 77656 Offenburg, Germany

[2] Albert-Ludwigs-Universität Freiburg, Technische Fakultät, Institut für Mikrosystemtechnik Büro: Geb. 106, 4. OG, Raum 015, Georges-Köhler-Allee 106, 79110 Freiburg, Germany

lukas.stiglmeier@hs-offenburg.de

Summary: This contribution introduces a guideline for the fabrication of fully 3D-printed torque sensor elements. Recent advances in 3D printing technology have made it possible to produce objects and functional structures by employing a variety of 3D printing processes and materials. 3D printing therefore provides an alternative approach to sensor fabrication. Fully 3D-printed resistive torque sensors, encompassing both the elastic structure and strain gauges produced by 3D printing processes, are rarely encountered in the literature. Here, we address this gap by presenting a guideline for the fabrication of fully 3D-printed torque sensor elements. The application of the guideline is demonstrated through a prototype. The guideline consists of three main steps: "Design", "Fabrication" and "Evaluation". As part of the guideline, the combination of different 3D printing materials and 3D printing processes will be demonstrated. In order to coordinate the different printing processes and materials, an iterative process is introduced in the design phase. In the second step, "Fabrication", the capabilities of a five-axis 3D printing system are demonstrated. In the final step, "Evaluation", the sensor element is calibrated. The aim of this guideline is to provide an orientation for the future development and research of 3D-printed sensor elements.

Keywords: guideline, 3D printing, torque sensor, fabrication, real example

Introduction

Additive Manufacturing, commonly known as 3D printing, has gained attention in the last years [1]. Numerous 3D printing processes do not only enable to fabricate bodies but also functional structures [2]. This offers potential in sensor manufacturing for detecting different physical quantities. In industrial applications, torque is a critical parameter. A variety of different sensing principles can be employed such as inductive, capacitive or resistive effects for torque measurement. The resistive effect, commonly implemented through strain gauges, is frequently applied. In this scenario, strain gauges are attached to an elastic structure that get deformed under torque. The resulting strain alters the electrical resistance of the strain gauge [3]. Recent scientific achievements demonstrate an alternative fabrication approach for both elastic structures [4–8] and strain gauges [9–12], employing additive manufacturing processes. The examination of the current research status reveals that the elastic structure of the torque sensors is often fabricated applying 3D printing processes. Commercially available strain gauges or optoelectronic components are then integrated onto these structures as sensor elements. Fully 3D-printed resistive torque sensors, where both the elastic structure and the strain gauge are manufactured, are rarely found in the literature. In this contribution, we resent a guideline for fabrication of such fully 3D-printed torque sensor elements to address this research gap. The guideline is illustrated with a practical example employing the resistive effect.

In the current literature, there are few guidelines for fabricated 3D-printed sensors. Schmitz et al. present a guideline for capacitive touch sensors in [13]. The guideline consists of the steps "3D Modelling", "Designing Interactivity", "3D Printing" and "Applications". A multi-material 3D printer applying fused layer modelling (FLM) is proposed for the fabrication of the sensors. The combination of different 3D printing processes is not addressed. The literature also provides general design guidances for 3D printing. These relate, for example, to the positioning of components in the build space [14].
No guidelines have been found in the current literature for the fabrication of 3D-printed torque sensor elements applying a combination of several 3D printing processes and conventional processes. The proposed guideline is made up of parts of the design concept for sensors presented in [15] and design rules for 3D printing.

Guideline for sensor development

The general process consists of three main steps. The first step is "Design". In this step, the CAD model and a mathematical model of the planned sensor element are created. The 3D printing materials and processes are also selected. The fabrication of the sensor element then takes place in the second step. After the physical production, the sensor element is evaluated in the final step, focusing on calibration of the sensor element. In the following sections, the three steps are explained in more detail using an example. Fig. 1 shows the three main steps.

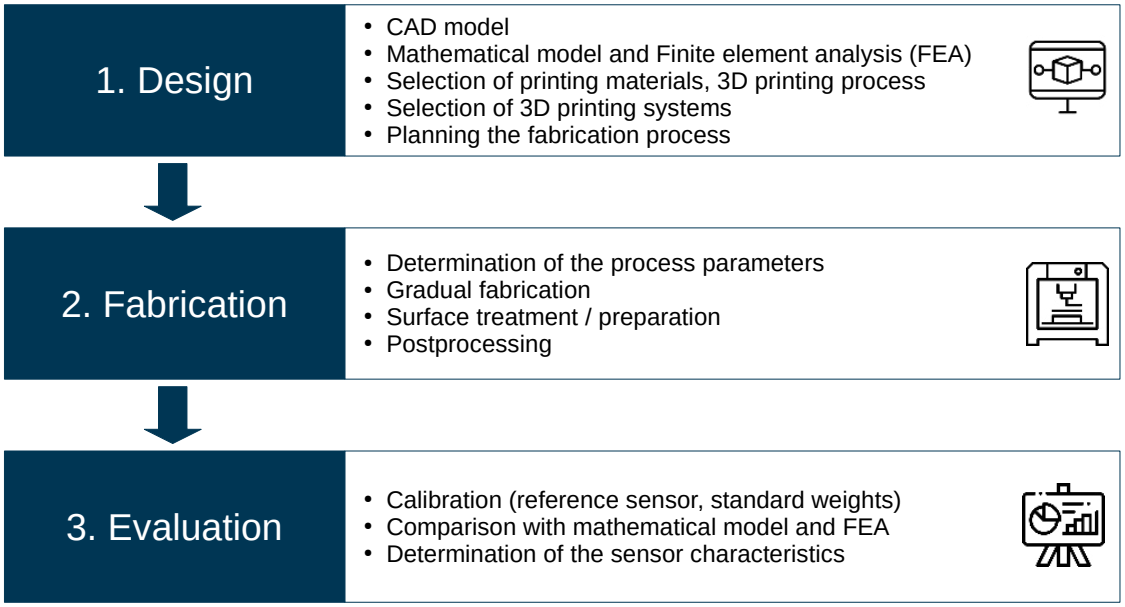

Fig. 1: Guideline for the fabrication of fully 3D-printed sensor elements.

Design

The first step, ”Design”, consists of several substeps that together form an iterative process. (Fig. 2). The iterative process is necessary to take into account the information gained during the design step.
CAD-Model: Once the idea and requirements have been defined, the sensor element concept is visualised applying a CAD model. This model incorporates the geometry tailored for the intended application. The CAD model also serves as the input for finite element analysis (FEA) and 3D printing. In this contribution, the ”example sensor element” depicted comprises a cylinder wrapped with conductive structures, as strain gauges (Fig. 3). This cylindrical design is suitable for integration into drive trains, among other applications. During production, M4 threaded inserts can be fused in, to facilitate flexible mounting of the sensor element. The second component of the sensor element comprises the conductive structures. Their electrical resistance changes under the influence of deformation. Conceptually, these structures resemble large strain gauges that encircle the entire circumference of the cylinder. The orientation of these structures is set at 45° to the shaft axis, as this angle corresponds to the orientation of the greatest strains during torsion [16]. At 90° to each other, two conductive structures are attached to the shaft. This configuration enables the utilization of the differential principle for torque measurement. Once the sensor element has been visualised, the next step is to create both a mathematical model and a FEA. The models provide information about the physical properties of the sensor element. It is also possible to analyse how changes in geometry and material parameters affect the sensor element.
Mathematical model: In general terms, ”[...] torsion means a twisting of a component around its longitudinal axis” [17]. Consequently, shear stress τ arises within the component. In correlation with shear γ and shear modulus G, Hooke's law for shear can be formulated as [17]

$$\tau = G \cdot \gamma. \tag{1}$$

Examining a cylinder, torsion increases linearly from the pole to the outer surface. Consequently, the highest shear stresses transpire at the surface of the cylinder. The extent of the final deformations of the cylinder depends, among other factors, on the geometry of the twisted object. Utilizing the torsional torque M_t and the polar moment of inertia W_p, the maximum shear stress τ_{max} can be computed applying [17]

$$\tau_{max} = \frac{M_t}{W_p}. \tag{2}$$

Focusing on the maximum shear stress, equations (1) and (2) can be combined to [17]

$$\gamma = \frac{M_t}{W_p \cdot G}. \tag{3}$$

Due to the later print orientation and the ’concentric circles’ infill pattern, the cross-sectional geometry of the cylinder consists of several thin-walled circles. The second polar moment of area W_p of a thin-walled circle is calculated according to equation (4), where r_o is the outer radius and r_i the inner radius of the shaft [17]. The effective polar moment of inertia can then be approximated by adding the individual polar moments of

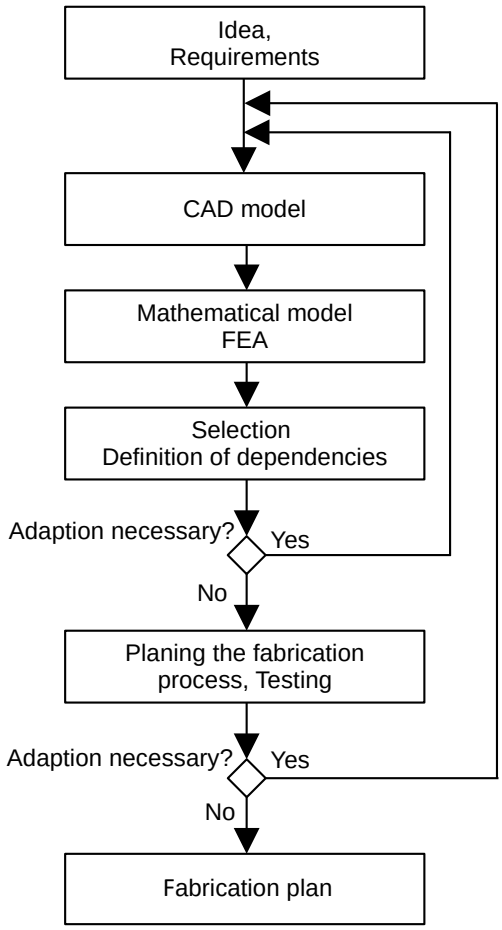

Fig. 2: Iterative process in the design step.

inertia of concentric circles.

$$W_p = \frac{\pi}{2} \cdot \frac{{r_o}^4 - {r_i}^4}{r_o} \tag{4}$$

In the next step, the connection to the occurring strains must be established. A rectangular surface element on the cylinder surface is considered for the derivation (Fig. 4). As a result of the shear deformations, the rectangle changes into a parallelogram. This means that strains occur in diagonal directions. The strains ϵ_1 and ϵ_2 then result with equations in [16]

$$\epsilon_1 = \gamma \frac{1}{2} \sin 2\alpha \tag{5}$$

$$\epsilon_2 = -\gamma \frac{1}{2} \sin 2\alpha. \tag{6}$$

Based on the derived strain, the change in resistance ΔR can now be determined with equation (7). Here, R is the original electrical resistance and k is the k-factor, which determines the sensitivity of the strain gauge [18]

$$\frac{\Delta R}{R} = \epsilon \cdot k. \tag{7}$$

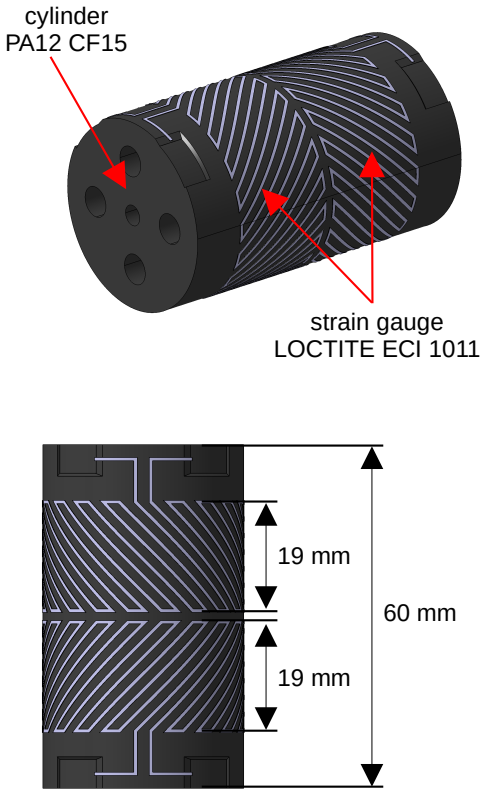

Fig. 3: CAD model of the developed sensor element.

The explanation from [18] is used to derive k. The starting point is the relationship described in equation (8) between the change in length and the resulting change in resistance. A is the cross-sectional area of the conductor and l is the length of the conductor. ζ depends on the material and is the specific electrical resistance. In this article, the geometry of a rectangle with edge lengths a and b is assumed for the cross-section of the conductive structures.

$$R = \zeta \cdot \frac{l}{A} = \zeta \cdot \frac{l}{a \cdot b} \tag{8}$$

The change in resistance ΔR can be estimated using the total differential

$$\Delta R = \frac{\partial R}{\partial \zeta} \Delta\zeta + \frac{\partial R}{\partial l} \Delta l + \frac{\partial R}{\partial a} \Delta a + \frac{\partial R}{\partial b} \Delta b. \tag{9}$$

After forming the total differential, an expression for the k-factor can be set up (10).

$$\frac{\Delta R}{R} = \frac{\Delta l}{l} \cdot \left(1 - \frac{\frac{\Delta a}{a}}{\frac{\Delta l}{l}} - \frac{\frac{\Delta b}{b}}{\frac{\Delta l}{l}} + \frac{\frac{\Delta \zeta}{\zeta}}{\frac{\Delta l}{l}}\right) \tag{10}$$

The expression for k is often given by equation (11). μ is the Poisson's ratio. It is assumed that the Poisson's ratio is the same for both edges of the rectangular cross-section. η is the relative

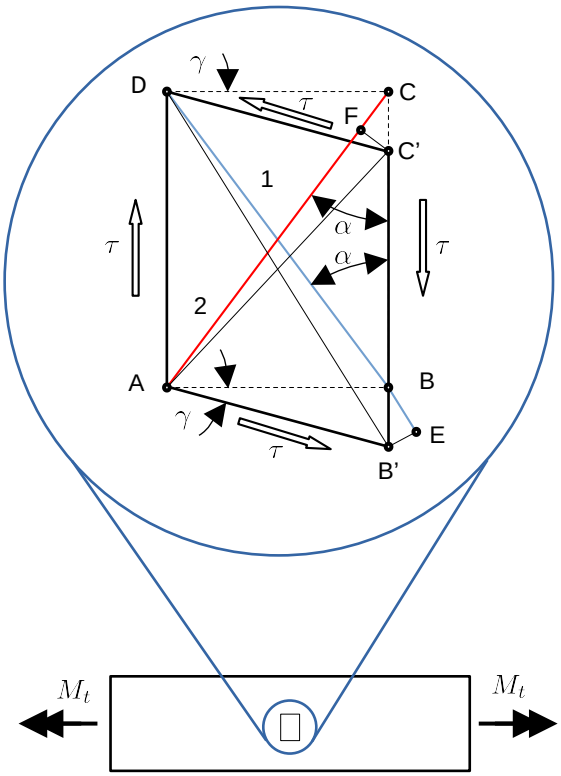

Fig. 4: Rectangular surface element on the cylinder surface (own presentation based on [16]).

change in specific electrical resistance due to the strain experienced.

$$k = 1 - \frac{\frac{\Delta a}{a}}{\frac{\Delta l}{l}} - \frac{\frac{\Delta b}{b}}{\frac{\Delta l}{l}} + \frac{\frac{\Delta \zeta}{\zeta}}{\frac{\Delta l}{l}} = 1 + 2\mu + \eta \qquad (11)$$

Strain gauges are typically analysed employing Wheatstone bridges. The design of the sensing element allows the use of a half bridge configuration. For this configuration, the relative bridge voltage can be determined applying equation (12). Where U_B is the bridge voltage, U_0 is the supply voltage to the measuring bridge, ϵ is the strain occurring in the strain gauges and k is the sensitivity of the strain gauges. A k-factor of 3.74 is assumed for the purposes of this paper. This has been determined from previous measurements.

$$\frac{U_B}{U_0} = \frac{1}{2} \cdot \epsilon \cdot k = \frac{1}{2} \cdot \frac{\Delta R}{R} \qquad (12)$$

FEA: FEA serves as a tool to validate the mathematical model. The simulation software *COMSOL Multiphysics*, applying the *Solid Mechanics* module is used to simulate the sensor element. Material parameters utilized in both the FEA and the mathematical model are enumerated in Tab. 1. The values are based on

Tab. 1: Mechanical and electrical properties of the materials

Description	Value	Unit
PA12 CF 15 Young's modulus	2190	MPa
ECI 1011 Young's modulus	10	MPa
PA12 CF15 Possion's ratio	0.36	-
ECI 1011 Possion's ratio	0.4	-
PA12 CF15 Density	1070	kg·m^{-3}
ECI 1011 Density	3000	kg·m^{-3}

information from data sheets. Fig. 5 illustrates the visual output, depicting the Von Mises stress at 3 N·m. It is evident that the highest stresses, and consequently strains, occur at the position of the conductive structures.

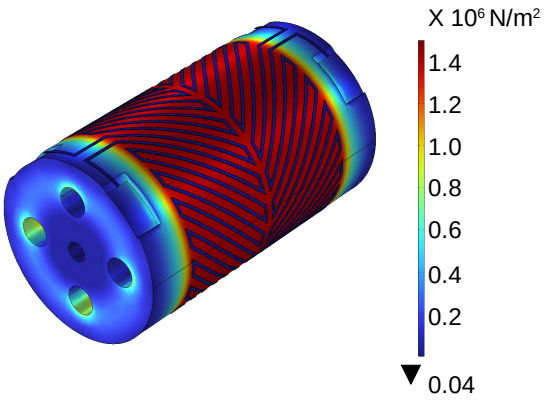

Fig. 5: Simulation result of the mechanical stresses of the sensor element at a torque of 3 N·m.

Selection: Following the iterative process (Fig. 2), this step involves the final selection of materials and 3D printing systems. The choice of 3D printing materials is influenced by a number of factors. First and foremost are the requirements, such as measurement range or sensitivity. The developed models can be used to virtually test different materials. The environmental conditions where the sensor will be used also play a role. These include the temperature or humidity at the location. The selection of 3D printing materials is determined not only by the previously defined requirements, but also by the dependencies resulting from the 3D printing materials. This aspect includes possible post-processing such as thermal curing. As a result, several iterations may be required before a

suitable combination of materials is found.
There are a large number of different 3D printing processes, which in turn allow a large number of different 3D printing materials to be processed. A widely employed 3D printing process is FLM. A plastic wire is melted through a nozzle and then selectively applied to the printing platform. The part is then built up layer by layer [1]. In this example, the cylinder will also be produced using FLM. Polylactic acid (PLA) or ABS are often used for FLM [19]. PLA has a Young's modulus of 3500 $N{\cdot}mm^{-2}$ (tensile test) and a temperature resistance of 55 °C [20]. In comparison, ABS has a Young's modulus of 1750 $N{\cdot}mm^{-2}$ (tensile test) and a temperature resistance of 85 °C [21]. In the context of this contribution, the sensor element is to be made more robust. Therefore nylon PA12 CF15 was chosen as the printing material. The material consists of polyamide (PA) as the basic matrix and discontinuous carbon fibres as the fibre reinforcement. The reasons for choosing this material is firstly the mechanical properties of the fibre reinforced material. The material has a higher Young's modulus (7300 $N{\cdot}mm^{-2}$ (tensile test)) compared to PLA and ABS. This Young's modulus is perpendicular to the direction of layer build-up. Due to the layered structure, 3D-printed objects exhibit anisotropic properties [14]. The Young's modulus in the direction of the layer structure is therefore lower. Another reason for choosing this material is its dimensional stability over temperature. According to the filament manufacturer, this is 150 °C [22]. This means that the sensor element can be used in a wider temperature range. The temperature resistance of the material is also crucial for the realisation of the strain gauges.
The strain gauges are applied to the cylinder surface applying Henkel's conductive ink *LOCTITE ECI 1011* using the PiezoJet process. This ink has been specially developed for flexible circuit boards. As a result, such structures can withstand mechanical deformations such as stretching without damage. This is the basis for the application of the resistive measurement principle. The ink requires a curing temperature of 150 °C to become conductive [23]. Due to the temperature resistance of PA12 CF15, thermal curing can be carried out without causing any damage to the 3D printed cylinder.
In total, two 3D printing systems are required to produce the sensor element. The cylinder is printed using the *MK3S* 3D printer from *PRUSA*. The conductive structures are printed on the *15XSA* multi-process 3D system from *Neotech AMT*. A special feature of the 3D printing system is the so-called five-axis operation. Commercially available 3D printers usually work with a cartesian coordinate system, consisting mainly of the X, Y and Z axes. In contrast, the *15XSA* 3D printing system has additional A and B axes that allow the printing platform to rotate. The five-axis operation allows printing on three-dimensional surfaces. Without this functionality, the realisation of the sensor element would be complex. In addition to five-axis operation, multiple machining processes can be integrated into the 3D printing system at the same time. This means that different 3D printing processes can be combined with conventional machining processes such as milling or a pick-and-place process.
As described in this section, there are a number of aspects to consider when selecting printing material. These include the properties of the sensor, the environmental conditions at the point of use and production-related aspects such as the curing temperature. The selection of print materials may, therefore, require several iterations of the design step (Fig. 2).
Planning the manufacturing process: The fabrication of the sensor element consists of several steps. In the first step, the cylinder is manufactured employing the FLM process with Nylon PA12 CF15 as the material. The cylinder is printed in an upright position to ensure a flat surface for printing the conductive ink. The resulting reduction in mechanical properties is partially compensated by the fibre reinforcement. After printing, the cylinder is removed from the build platform and prepared for ink application. The first step is to melt four M4 threaded inserts into each side of the cylinder, which act as mounting fixtures in torque transmission. The subsequent procedure involves preparing the surface of the cylinder for the application of conductive ink. Owing to its layered structure, the cylinder surface is rough. The cylinder is rolled to achieve a smoother surface. The rolling tool is heated to induce softening of the material on the surface. Copper pads are also bonded to the cylinder for contact. After surface preparation, the conductive structures are 3D-printed using Henkel's *LOCTITE ECI 1011* silver ink. A *Nordson* PiezoJet print head is chosen to apply the silver ink. The PiezoJet print head works on the basis of the inverse piezoelectric effect, in which a piezoelectric material is excited by an alternating voltage, causing it to deform at the frequency of the alternating voltage [24]. This actuator, which is mechanically connected to a plug that acts as a valve on the nozzle, moves up and down in response to the excitation, ejecting the print material from the nozzle as droplets. Once the ink has been printed, the entire sensor element is thermally treated in an oven at 140 °C for 20 minutes. Previous tests have shown that the ink cures sufficiently at 140 °C and has usable conductivity. The ink was cured at 140 °C to avoid irreversible deformation of the 3D-printed cylinder. Finally, the measurement leads are soldered to the copper pads. The planned production process is shown in Fig. 6.
During the planning phase, new information may emerge that requires a redesign of the sensor element, thus initiating the iterative process in the design step (Fig. 2). Printing tests can

also be useful to identify potential limitations at an early stage. The redesign may affect the characteristics of the sensor element, so all models will need to be adjusted.

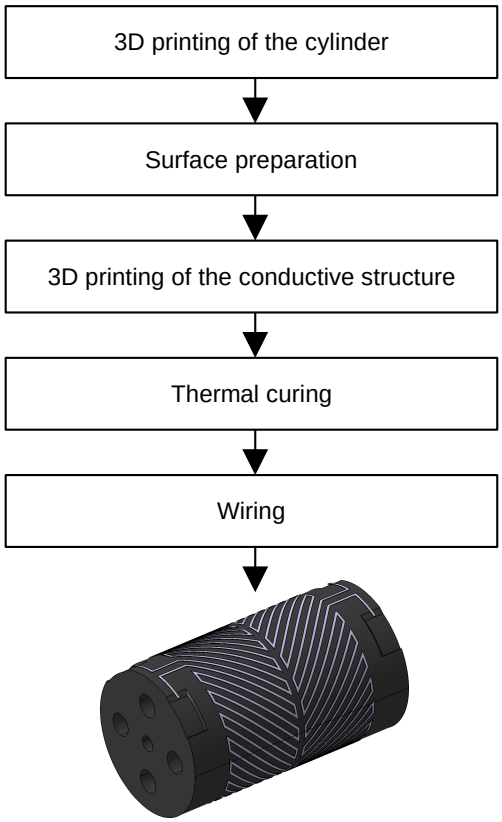

Fig. 6: Planning the fabrication process.

Fabrication of the sensor element

The sensor element is manufactured following the provided fabrication plan. This section outlines the key steps involved. Initially, the surface treatment of the cylinder for ink application is conducted. The cylinder undergoes manual rolling using a heated foil iron. Fig. 7 illustrates the cylinder surface before and after treatment. It is evident that on the untreated cylinder surface, the ink seeps into the crevices between the printed layers. An even conductive pattern cannot be achieved, leading to an irreproducible resistance of the conductive pattern.
The conductive structures are applied to the cylinder surface using the PiezoJet process in conjunction with five-axis operation. This necessitates an adapter between the printing platform and the cylinder, which is also fabricated from PA12 CF 15 using FLM. The brackets are employed to elevate the print platform and are indispensable for five-axis operation. The process parameters for the piezojet process vary depending on the materials utilized. Hence, testing

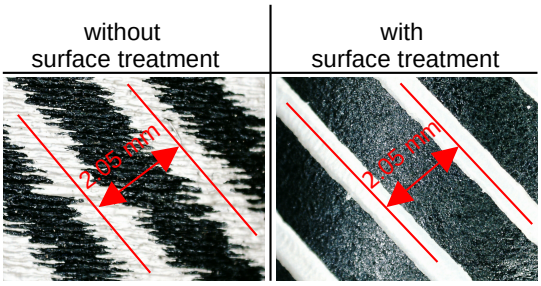

Fig. 7: Surface treatment of the cylinder for the ink printing.

was conducted to ascertain these parameters before the final printing of the sensor element. Upon determining the final process parameters, the conductive structures are generated. Fig. 8 depicts the 3D printing system applying the ink in five-axis mode. The cylinder rotates beneath the print head, facilitating the creation of the strain gauge structure. After printing of the ink, the entire sensor element undergoes thermal treatment in an oven at 140 °C for 20 minutes. The fabricated sensor element is shown in Fig. 9.

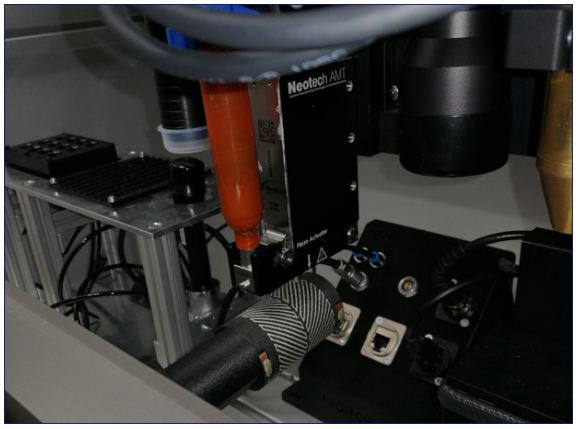

Fig. 8: Fabrication of the sensor element during five-axis operation.

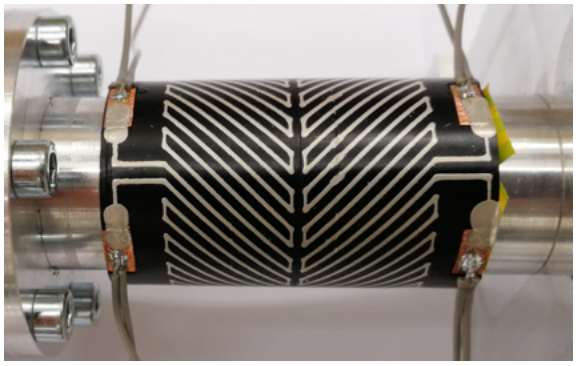

Fig. 9: Fabricated sensor element.

Evaluation

Following the guideline, the final step is to evaluate the sensor element in terms of its metrological properties.
Calibration: The first step involves calibration, aimed at establishing the relationship between the measured variable and the output variable. Initially, the resistances of the conductive structures are measured employing the *Keithley 2450 Sourcemeter* digital multimeter. The recorded resistances are 6.38 Ω (s = 0.77 mΩ) for the first strain gauge and 6.42 Ω (s = 0.32 mΩ) for the second.
A customized test stand is utilized to further calibrate the produced "example sensor element" (Fig. 10). This test stand comprises a metal plate serving as the base, with three bearings mounted on it. The sensor element is affixed to the right side of the test stand, whereas the two bearings on the left allow rotation of the shaft around the central axis. The shaft is linked to a lever arm to apply defined torques to the sensor element. Controlled forces are applied to the lever arm using the *lbr iiwa* robot. This robot features torque sensors in the joints to exert controlled forces. Burster's *8431* force sensor is affixed to the robot flange to monitor the forces. Due to the low resistance of the printed strain gauges, a 120 Ω resistor is connected in series with each strain gauge. The structures, along with the series resistors, are interconnected to form a Wheatstone bridge in a half-bridge configuration. *HBM*'s *Quantum X MX440A* amplifier is employed to measure the bridge voltage.

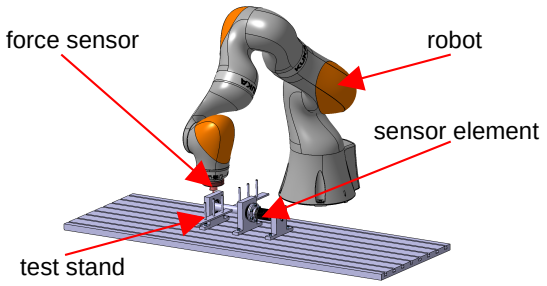

Fig. 10: Test stand for calibrating the sensor element.

The measured values are then compared with both the mathematical model and the FEA. Fig. 11 shows the relative bridge voltage as a function of the acting torques. When comparing between the values from the mathematical model and the values from the FEA, a maximum deviation of 3.12 % can be observed here. The deviation can be attributed to the simplification in the mechanical calculation. The maximum difference between the simulated and measured values in the range from -3 N·m to 3 N·m is 21.71 % and between the mathematical model and the measured values is 18.03 %.
The measurement results (torque and relative bridge voltage) are almost proportional to each other. This is shown by the linear regression. Fig. 12 shows the measured values together with the regression line. This gives a coefficient of determination of R^2= 0.9940.

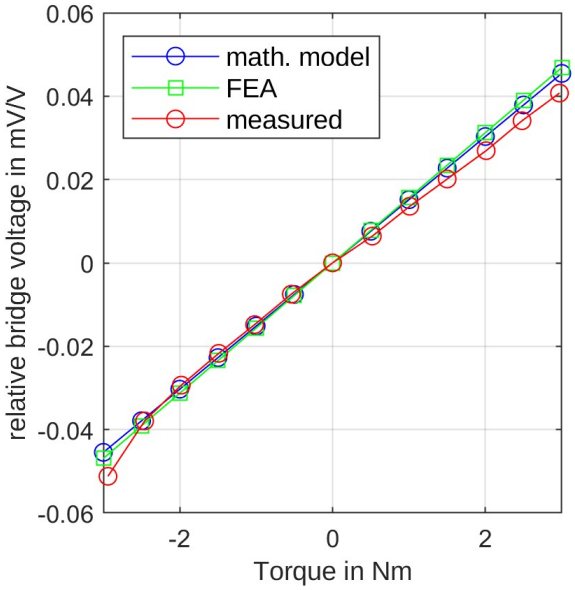

Fig. 11: Comparison of the measured values with the mathematical models and FEA.

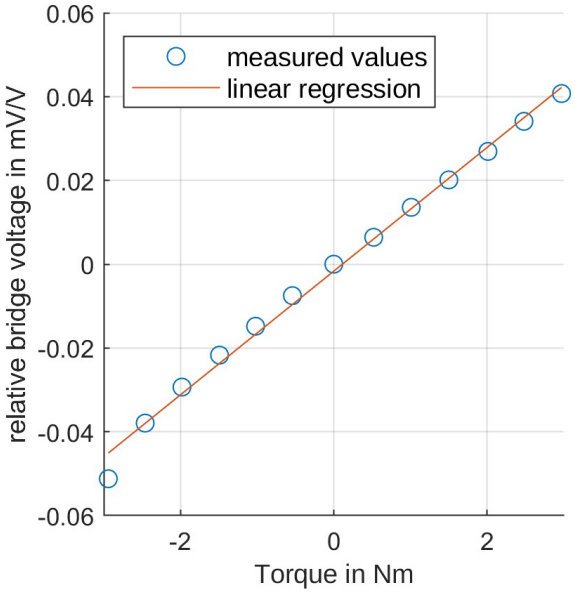

Fig. 12: Behaviour of the sensor element with regard to linearity.

Conclusion and outlook

Following the guideline provided, a sensor element for torque detection was modeled, simulated, manufactured, and verified. The measurement results confirmed those obtained from

the previous calculations and simulations. Small discrepancies between the calculated and simulated values can be attributed to simplifications in the mechanical calculations. Furthermore, the results validate the practicality of the guideline. A crucial aspect is coordinating the various printing materials and the resulting dependencies. An iterative process was set up in the design step to coordinate them. Additionally, the potential of a five-axis 3D printing system for ink application was demonstrated, highlighting its ability to streamline the process by directly printing the ink, thus replacing the time-consuming task of gluing strain gauges. The guideline provides a systematic approach for the future development and research of 3D-printed sensing elements.

Acknowledgment

Funded by the Deutsche Forschungsgemeinschaft (DFG, German Research Foundation) – 426605889

References

[1] Uwe Berger, Andreas Hartmann, and Dietmar Schmid. *3D-Druck - Additive Fertigungsverfahren: Rapid Prototyping, Rapid Tooling, Rapid Manufacturing*. Bibliothek des technischen Wissens. Verlag Europa-Lehrmittel - Nourney Vollmer GmbH & Co. KG, Haan-Gruiten, 2. auflage, mit bilder-cd edition, 2017.

[2] Mohammad Reza Khosravani and Tamara Reinicke. 3d-printed sensors: Current progress and future challenges. *Sensors and Actuators A: Physical*, 305:111916, 2020.

[3] Rainer Schicker and Georg Wegener. *Drehmoment richtig messen*. Hottinger-Baldwin-Messtechnik, Darmstadt, 2002.

[4] Liyue Fu, Aiguo Song, and Dapeng Chen. A polyetheretherketone six-axis force/torque sensor. *IEEE Access*, 7:105391–105401, 2019.

[5] Jiantao Yao, Hongyu Zhang, Ximei Xiang, Huidong Bai, and Yongsheng Zhao. A 3-d printed redundant six-component force sensor with eight parallel limbs. *Sensors and Actuators A: Physical*, 247:90–97, 2016.

[6] Daisuke Okumura, Sho Sakaino, and Toshiaki Tsuli. Miniaturization of multistage high dynamic range six-axis force sensor composed of resin material. 2019.

[7] Narciso Soto, Jose Garcia, Brittany Newell. Development of torque sensors using additive manufacturing. 2021.

[8] Alan Wang and Perry Y. Li. A 3d-printed low-cost 6-dof human interaction force sensor for a haptic interface. In *2021 IEEE/ASME International Conference on Advanced Intelligent Mechatronics (AIM)*, pages 936–941. IEEE, 2021.

[9] V. Correia, C. Caparros, C. Casellas, L. Francesch, J. G. Rocha, and S. Lanceros-Mendez. Development of inkjet printed strain sensors. *Smart Materials and Structures*, 22(10):105028, 2013.

[10] Shweta Agarwala, Guo Liang Goh, and Wai Yee Yeong. Aerosol jet printed strain sensor: Simulation studies analyzing the effect of dimension and design on performance (september 2018). *IEEE Access*, 6:63080–63086, 2018.

[11] Michela Borghetti, Mauro Serpelloni, and Emilio Sardini. Printed strain gauge on 3d and low-melting point plastic surface by aerosol jet printing and photonic curing. *Sensors (Basel, Switzerland)*, 19(19), 2019.

[12] Dilan Ratnayake, Alexander Curry, and Kevin Walsh. Demonstrating a new ink material for aerosol printing conductive traces and custom strain gauges on flexible surfaces. In *2021 IEEE International Conference on Flexible and Printable Sensors and Systems (FLEPS)*, pages 1–4. IEEE, 2021.

[13] Martin Schmitz, Mohammadreza Khalilbeigi, Matthias Balwierz, Roman Lissermann, Max Mühlhäuser, and Jürgen Steimle. Capricate: A fabrication pipeline to design and 3d print capacitive touch sensors for interactive objects. In Celine Latulipe, Bjoern Hartmann, and Tovi Grossman, editors, *Proceedings of the 28th Annual ACM Symposium on User Interface Software & Technology*, pages 253–258, New York, NY, USA, 2015. ACM.

[14] Andreas Gebhardt, Julia Kessler, and Laura Thurn. *3D-Drucken: Grundlagen und Anwendungen des Additive Manufacturing (AM)*. Hanser eLibrary. Hanser, München, 2. edition, 2016.

[15] Hans-Rolf Tränkler and Leo Reindl. *Sensortechnik*. Springer Berlin Heidelberg, Berlin, Heidelberg, 2014.

[16] Klaus Agne. *Technische Mechanik in der Feinwerktechnik: Aufgaben, Beispiele, Lösungen*. Viewegs Fachbücher der Technik. Vieweg+Teubner Verlag, Wiesbaden, 3., verbesserte auflage edition, 1988.

[17] Ralf Bürgel. *Lehr- und Übungsbuch Festigkeitslehre: Mit 10 Tabellen ; [mit 114 Aufgaben und 63 Seiten Lösungen*, volume Bd. 1 of *Studium Technik*. Vieweg, Wiesbaden, 1. aufl. edition, 2005.

[18] Rainer Parthier. *Messtechnik*. Springer Fachmedien Wiesbaden, Wiesbaden, 2020.

[19] Andreas Fischer, Dirk Achten, and Martin Launhardt. *Kunststoff-Wissen für die additive Fertigung: Eigenschaften, Formulierung und Einsatzgebiete von Thermoplasten*. Hanser eLibrary. Hanser, München, 2023.

[20] Fiberlogy. Technical data sheet easy pla, 2022. `https://fiberlogy.com/de/filamente/easy-pla/` [Accessed: 18.04.2024].

[21] Fiberlogy. Technical data sheet abs, 2022. `https://fiberlogy.com/de/filamente/abs/` [Accessed: 18.04.2024].

[22] Fiberlogy. Technical data sheet nylon pa12+cf15, 2021. `https://www.3djake.de/fiberlogy/nylon-pa12cf15`.

[23] Henkel. Loctite eci 1011 e&c, 2016.

[24] Stefan Johann Rupitsch. *Piezoelectric Sensors and Actuators: Fundamentals and Applications*. Topics in Mining, Metallurgy and Materials Engineering. Springer Berlin Heidelberg and Imprint: Springer, Berlin Heidelberg, 1st ed. 2019 edition, 2019.